2012

Effect of Condenser Subcooling of the Performance of Vapor Compression Systems: Experimental and Numerical Investigation

Gustavo Pottker
pega@illinois.edu

Predrag S. Hrnjak

Effect of Condenser Subcooling of the Performance of Vapor Compression Systems: Experimental and Numerical Investigation

Gustavo POTTKER, Pega HRNJAK*

Department of Mechanical Science and Engineering
University of Illinois at Urbana-Champaign
1206 West Green Street, Urbana, IL 61801, USA
* Corresponding Author: pega@illinois.edu

ABSTRACT

This paper presents a theoretical and experimental analysis of the effect of condenser subcooling on the performance of vapor-compression systems. It is shown that, as condenser subcooling increases, the COP reaches a maximum as a result of a trade-off between increasing refrigerating effect and specific compression work. The thermodynamic properties associated with the relative increase in refrigerating effect, i.e. liquid specific heat and latent heat of vaporization, are dominant to determine the maximum COP improvement with condenser subcooling. Refrigerants with large latent heat of vaporization tend to benefit less from condenser subcooling. For a typical AC system, numerical results indicate that the R1234yf would benefit the most from condenser subcooling in comparison to R410A, R134a and R717 due to its smaller latent heat of vaporization. On the other hand, the value of COP maximizing subcooling does not seem to be a strong function of thermodynamic properties. Experimental results comparing R1234yf and R134a confirmed the trends observed during the numerical study. For a given operating condition, the system COP increased up to 18% for R1234yf and only 9% for R134a.

1. INTRODUCTION

The state of the refrigerant entering the expansion device of conventional vapor compression cycles is usually assumed to be saturated liquid. However, liquid cooling below saturation reduces the throttling losses and potentially increases COP. Subcooled liquid prior to expansion process can be obtained by adding extra components such as internal heat exchangers in single-stage cycles (Domanski and Didion, 1994) and in two-stage cycles. Subcooling can also be achieved by an auxiliary cooling system such as a thermoelectric device (Radermacher et. al., 2007), a secondary vapor compression system – also known as mechanical subcooling (Couvillion et. al., 1988) or using available coolant supplies, such as condensate water from evaporator (Peterson, 1997).

An additional heat-sink cooled heat exchanger, usually denominated subcooler, can also be used to obtain subcooling. Typically, a high-side pressure receiver is installed between the condenser and the subcooler in order to separate liquid from vapor before liquid runs through the subcooler. One can think of the subcooler not only as separate heat exchanger but as part of a then larger condenser which has some of its surface allocated to subcool liquid. In fact, the most conventional way to obtain subcooling in systems without a liquid receiver is by utilizing part of condenser heat transfer area to cool down the liquid below the saturation temperature. Rather than in a high-side pressure receiver, the liquid-vapor interface is eliminated inside the tubes of the condensers, as liquid refrigerant accumulates towards the exit of the heat exchanger. The so-called condenser subcooling is typically obtained during a refrigerant charging procedure. The question raised by Gosney (1982) is whether one would be better off using the subcooling heat transfer surface, either within the condenser or in a separate subcooler, to reduce the condensing pressure and consequently the compression work.

Linton et al. (1992) experimentally investigated the effect of condenser liquid subcooling on a refrigeration system performance. Results showed that the cooling COP and refrigeration capacity of all three refrigerants benefited from subcooling increase (from 6°C to 18°C): R134a (12.5%), R12 (10.5%) and R152a (10%), while condensing temperature was kept artificially constant. Subcooling has also been subject of publications related to automotive air conditioners. These systems are usually equipped with either a high-side liquid receiver or a low-side accumulator in order to absorb fluctuations in refrigerant charge. Yamanaka et al. (1997) presented a concept of a sub-cool system in which the liquid receiver is installed before the last pass of a parallel flow microchannel condenser rather than at the exit of the condenser. COP would benefit from subcooling due to an increase in enthalpy difference across

evaporator. Condensers with integrated receiver and subcooler pass have become standard in state-of-the-art automotive air conditioning systems. Pomme (1999) also presented a similar study in which subcooling was generated by a pre-expansion valve between the condenser exit and the liquid receiver.

A few publications that examined the influence of the refrigerant charge on the COP indirectly explored the relationship between subcooling and COP. Corberan et al. (2008) maximized COP by varying the refrigerant charge in an R290 heat pump equipped with a thermostatic expansion valve. They explained that the system responded to increasing charge by rising the condenser subcooling since no receiver was installed. The COP maximizing charge was related to a COP maximizing subcooling. Primal and Lundqvist (2005) had also optimized the charge of a R290 domestic water heat pump and found the corresponding subcooling to be 4-5°C.

Although condenser subcooling is a practical issue in the everyday of refrigeration and air conditioning systems, to the best of authors' knowledge, this topic has not been the subject of a systematic study in the open literature so far. This study is an attempt to start filling up this gap. First, this paper will theoretically explore the performance trade-off associated with condenser subcooling using cycle analysis. Then, important thermodynamic properties related to this trade-off will be identified and a sensitivity analysis will be presented for different refrigerants. Second, a comprehensive simulation model of an air conditioner will be used estimate potential for COP improvement with condenser subcooling for different refrigerants. Finally, the effect of subcooling on the performance of an actual vehicular air conditioning system will experimentally investigated for two refrigerants (R134a and R1234yf) under the same operating conditions.

2. CYCLE ANALYSIS

Fig. 1 illustrates a schematic of a water-cooled tube-in-tube condenser with and without subcooling and Fig. 2 outlines the respective cycles on a T-h diagram. A prime (') denotes the cycle with subcooling. Due to the presence of subcooled liquid (Fig 1b), the two-phase heat transfer area would be reduced relative to a condition without subcooling (Fig 1a). As a result, the saturation temperature would rise in the condenser ($\Delta T_{c,sat}$, Fig. 2) which would subsequently increase the specific compression work (Δw, Fig. 2). On the other hand, the refrigerant temperature at the condenser outlet would decrease ($\Delta T_{c,out}$, Fig. 2), increasing subsequently the refrigerant enthalpy difference through the evaporator (Δq, Fig. 2). This logic can be expressed by Eq. (1) and suggests that COP may undergo a maximum, resulting from a trade-off between increasing specific refrigerating effect (by Δq) and compression work (by Δw). As illustrated in Fig. 2, strictly speaking, the subcooling ($\Delta T_{c,sub}$) can be a result of both a decrease in refrigerant condenser exit and an increase in condensing temperature.

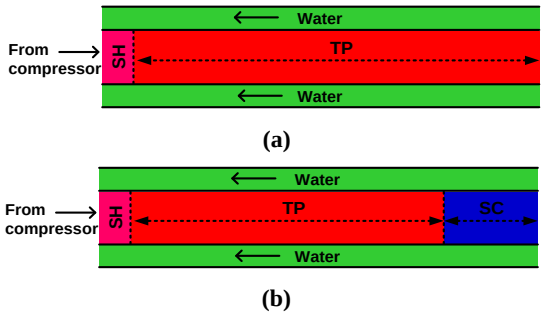

Figure 1: Schematic of a water-cooled condenser with (a) and without (b) subcooling.

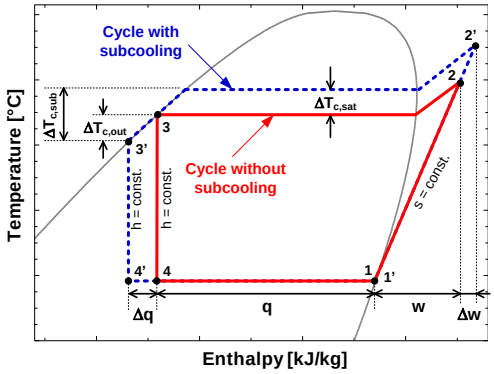

Figure 2: Schematic of cycles with and without subcooling in a T-h diagram.

$$COP' \approx COP\left(1+\frac{\Delta q}{q}-\frac{\Delta w}{w}\right) \tag{1}$$

$$COP=\frac{q}{w} \tag{2}$$

The relative increase in refrigerating effect ($\Delta q/q$) can be approximated by Eq. (3) which shows that the relative change in refrigerating effect due to the variation of the refrigerant outlet temperature to the condenser depends on the ratio of liquid specific heat to latent heat of vaporization and on the temperature lift, $(T_c - T_e)_{sat}$. It suggests that reducing the temperature of the refrigerant at the condenser exit would be more welcome for refrigerants with large

liquid specific heat and smaller latent heat of vaporization and for operating conditions with high temperature lifts. A similar approach is taken for the relative increase in specific isentropic compression work ($\Delta w/w$), given by Eq. (4).

$$\frac{\Delta q}{q} = \frac{\Delta T_{c,out}}{\frac{h_{fg,e}}{\bar{c}_{pl}} + \left(T_c - T_e\right)_{sat}} \tag{3}$$

$$\frac{\Delta w}{w} = \left(\frac{h_{2'} - h_2}{h_2 - h_1} \right)_{is} \tag{4}$$

Table 1 shows calculated numerical values of $\Delta q/q$ and $\Delta w/w$ for several refrigerants, with fixed $\Delta T_{c,out}$ = 5°C and $\Delta T_{c,sat}$ = 1°C. The evaporation temperature was fixed at 5°C. The condensing temperature was fixed for the baseline non-subcooled cycle at 45°C. It can be observed in Table 1 that the R404A is the refrigerant with the highest potential gain in refrigerating effect (8.3%) due to a small latent heat of vaporization (161 kJ/kg), even though the liquid specific heat (1.6 kJ/KgK) is not high relative to other fluids. The second largest $\Delta q/q$ is from R1234yf (7.4%), about 1.9% larger than R134a, also due to a narrow latent heat of vaporization. Several widely used refrigerants such as R410A, R290, R600a, R134a and R407C are within a range of 5.3% to 6.4%. Besides their high liquid specific heats, R717 and R718 have low potential to gain refrigerating effect due to a very large latent heat of vaporization. Regarding the increase in compression work ($\Delta w/w$), all fluids behave similarly within a range of 1.9% to 2.8%, with R717 and R718 having the highest sensitivity to increase in condensing temperature.

Table 1: Effect of refrigerant properties on the relative increase in refrigerating effect and specific isentropic compression work

Refrigerant	$c_{pl,c}$	$h_{fg,e}$	$\Delta q^*/q$	$\Delta w^{**}/w$
[-]	[kJ (kg K)$^{-1}$]	kJ kg^{-1}	[%]	[%]
R11	0.9	187	2.9	2.3
R12	1.0	149	4.6	2.2
R1234yf	1.5	160	7.4	2.1
R134a	1.5	195	5.5	2.2
R152A	1.9	301	4.2	2.2
R22	1.6	200	5.3	2.3
R290	2.9	367	5.7	2.2
R404A	1.6	161	8.3	2.1
R407C	1.7	205	6.1	1.9
R410A	1.9	217	6.4	2.3
R600a	2.6	346	5.3	2.1
R717	5.0	1244	2.4	2.5
R718	4.2	2489	0.9	2.8

* based on $\Delta T_{c,out}$ = 5°C

** based on $\Delta T_{c,sat}$ = 1°C

Figs. 3 and 4 show the results for $\Delta q/q$ and $\Delta w/w$ as a function of condensing temperature for various refrigerants, considering a fixed $\Delta T_{c,out}$ = 5°C and $\Delta T_{c,sat}$ = 1°C, respectively.

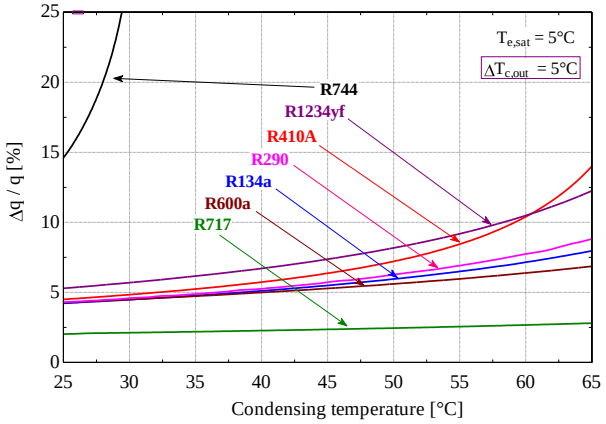

Figure 3: Effect of the condensing temperature on the relative gain in refrigerating effect for a $\Delta T_{c,out}$ = 5°C.

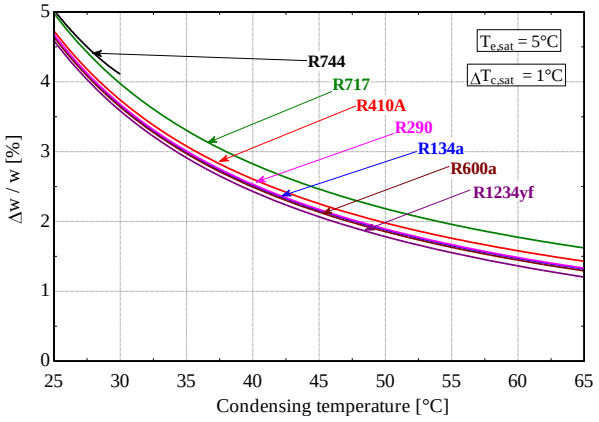

Figure 4: Effect of the condensing temperature on the relative increase in isentropic compression work for a $\Delta T_{c,sat}$ = 1°C.

In the low condensing temperature range (up to 30°C), it can be seen that the R744 is actually the refrigerant with the highest potential gain in refrigerating effect due a very small latent heat of vaporization combined with a high liquid specific heat associated with proximity to the critical point. In Fig. 3, for all refrigerants, as the condensing temperature increases and approaches the critical point, the liquid specific heat becomes higher and the latent heat of vaporization decreases, which subsequently increases the refrigerating effect gain (Eq. 3). An addition contribution

is given by higher temperature lifts, $(T_c - T_e)_{sat}$, that also increase with the condensing temperature since the evaporating temperature was fixed (Eq. 3). Regarding the increase in compression work (Fig. 4), it can be observed that all refrigerants become less sensitive to $\Delta T_{c,sat}$ at higher condensing temperatures, due to the increase in the temperature lift, $(T_c - T_e)_{sat}$.

Table 1 and Figs. 3 and 4 provided a simplified analysis of the effect of thermodynamic properties on the sensitivity of refrigerating effect and compression work to fixed increments in saturation ($\Delta T_{c,sat}$ = 1°C) and outlet ($\Delta T_{c,out}$ = 5°C) condenser temperatures. However, in order to determine the COP change due to subcooling, the actual values of $\Delta T_{c,sat}$ and $\Delta T_{c,out}$ must be obtained. These increments are inter-dependent due to heat transfer characteristics in refrigerant and secondary fluid sides. They can only be determined by numerically modeling or experimentally testing an actual condenser. Results from both approaches are analyzed next.

3. MODEL DESCRIPTION

A simulation comprehensive model was developed and programmed in EES (2007) for a conventional air conditioning system comprising air-to-refrigerant multi-pass cross-flow microchannel condenser and evaporator, a hermetic compressor and an expansion valve. A description of the heat exchangers is shown in Table 2 Condenser and evaporator characteristics are typical of those used in 3.5kW state-of-the-art residential air conditioning split systems. For all fluids of interest, the heat exchangers used in the simulation were the same in terms of refrigerant and air-side heat transfer areas.

Table 2: Detailed description of condenser and evaporator

	Condenser	Evaporator
Air side area (m^2)	14.01	8.42
Ref. side area (m^2)	1.54	0.92
Face area (m^2)	0.40	0.24
Depth (mm)	24	24
Fin spacing (mm)	1.27	1.27
Fin type/material	Louvered/Aluminum	
Tubes	2 x 24 mm / 40 tubes	
Ports (per tube)	12 x 0.8 mm (diameter)	

The system components were modeled separately in modules and linked through thermodynamic properties (enthalpy and pressure) and refrigerant mass flow rate. For the compressor, a fixed isentropic efficiency of 70% was assumed for all refrigerants. In addition, it was assumed that 15% of the input power to the compressor was lost by heat rejection through the shell, with the remaining 85% being absorbed by the refrigerant. An isenthalpic expansion was assumed. The heat exchangers were modeled using a finite volume method. Each pass of the condenser was divided in 20 volumes. A total of 20 volumes were used in the evaporator.

Each finite volume contained the total number of tubes of the respective pass, since the refrigerant distribution in the headers was considered homogeneous. On the air side, uniform inlet temperature and velocity were also assumed. For each finite volume, the heat transfer rate and the refrigerant outlet enthalpy were calculated using the effectiveness-NTU method for a cross-flow heat exchanger with the two fluids unmixed. In order to determine the "UA" value of each finite volume, only refrigerant and air side convection resistances were considered. The fin efficiency was calculated according to Incropera et al. (2006). The refrigerant and air side heat transfer correlations used in the model are listed in Table 3. Fully dry conditions were assumed throughout the evaporator.

Table 3: Heat transfer and pressure drop correlations

Refrigerant condensation heat transfer coefficient	Cavallini (2006)
Refrigerant boiling heat transfer coefficient	Gungor and Winterton (1976)
Refrigerant single-phase heat transfer coefficient	Turbulent: Gnielinski (1976) Laminar: Analytical solution
Air side heat transfer coefficient and friction factor for louvered fins	Chang and Wang (1997)
Two-phase refrigerant pressure drop	Friedel (1979)
Single phase refrigerant pressure drop	Friction factor from Churchill (1977)

The refrigerant-side pressure drop in each finite volume was calculated from widely used friction factor correlations (Table 3) for major losses, while minor losses were neglected. Refrigerant-side pressure drop across connecting lines was also neglected. The input variables of the model are condenser and evaporator geometric parameters, inlet air temperature and velocity to the heat exchangers, refrigerant superheat at the evaporator outlet and subcooling at the condenser outlet as well as the system cooling capacity. Typical outcomes of the model are evaporating and condensing temperatures, refrigerant-side pressure drop through the heat exchangers and COP.

3. SIMULATION STUDY

In this section, the simulation model is used to evaluate the effect of subcooling on the overall system performance for different refrigerants. The operating conditions include outdoor and indoor air temperatures of 35°C and 27°C, respectively, air face velocity of 1.0 m/s in both heat exchangers, in addition to an evaporator exit superheat of 1°C.

Fig. 5 shows simulation results of the saturation and outlet temperatures in the condenser, while Fig. 6 presents the normalized COP, refrigerant enthalpy difference across evaporator and specific compression work, all as a function of the condenser subcooling. The fluid was R1234yf. For each condenser subcooling imposed to the simulation model, the cooling capacity was kept constant at 4 kW so that COP would be only measure of improvement. As subcooling increases, the saturation temperature in the condenser becomes higher due to the reduction of the two-phase region. In addition, the subcooling zone introduces an area of both lower air-refrigerant temperature difference and refrigerant-side heat transfer coefficient. As a result, specific compressor work increases (Fig. 6). On the other hand, the condenser exit temperature decreases, consequently increasing the enthalpy difference across the evaporator (Fig. 6). The trade-off between increasing compression work and refrigerating effect results in a maximum COP at a specific subcooling value (Fig. 6). This trade-off is physically different from that which determines whether an internal heat exchanger improves or not the COP of single-stage cycles. According to Domanski and Didion (1994), in single-stage internal heat exchanger cycles the increase in compression work is due to an increase in temperature and, subsequently, in specific volume at the compressor inlet, while in condenser subcooled cycles the compression work increases due to higher condensing pressures.

Besides the primary mechanism of improvement of the subcooling - lower temperature at the condenser exit – there may be secondary benefits such as decrease in refrigerant-side pressure drop. From zero to the COP maximizing subcooling, the refrigerant flow rate needed to match cooling capacity of 4 kW decreased by about 10% due to the increase in refrigerating effect. As a result, the refrigerant-side pressure drop in the evaporator dropped by 18%. In the condenser, both lower refrigerant flow rate and the presence of single-phase liquid contributed to a decrease in 54% in refrigerant-side pressure drop from zero to COP maximizing subcooling.

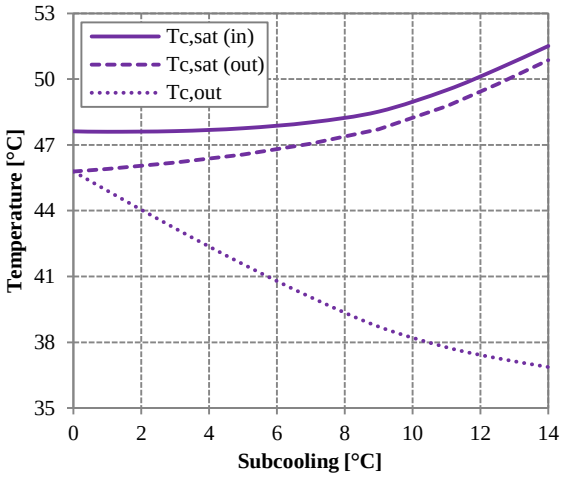

Figure 5: Effect of condenser subcooling on refrigerant temperatures at the condenser at outdoor and indoor temperatures of 35°C and 27°C (R1234yf)

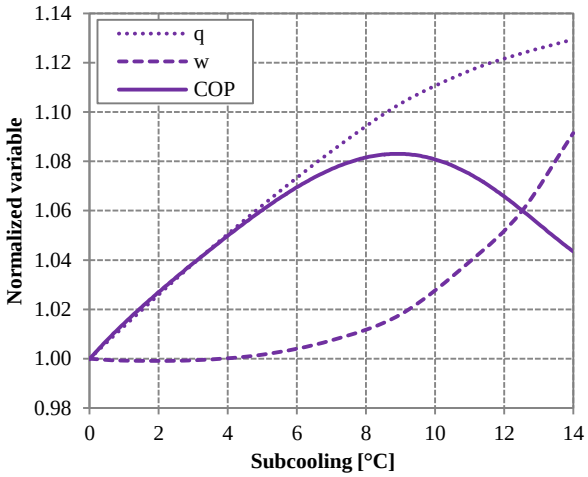

Figure 6: Effect of condenser subcooling on normalized COP, refrigerating effect and specific compression work at outdoor and indoor temperatures of 35°C and 27°C (R1234yf)

Fig. 7 shows the normalized COP as a function of the condenser subcooling for R1234yf, R410A, R134a and R717, while Table 4 summarizes the simulation results comparing the performance at zero versus that at COP maximizing subcooling. The cooling capacity was fixed at 4 kW and the operating conditions are the same as those in Figs. 5 and 6. It can be seen from Fig. 7 that the COP maximizing subcooling is roughly 9°C for all four refrigerants. However, the refrigerant properties affect the maximum COP increase. Within the four refrigerants, R1234yf showed the greatest COP improvement (8.4%) due to subcooling, followed by R410A (7.0%), R134a (5.9%) and R717 (2.7%).

Table 4 indicates that the dominant effect was the relative increase in evaporator enthalpy difference ($\Delta q/q$) from zero to optimum subcooling, while the relative increase in compression work ($\Delta w/w$) was much smaller. These improvements are consistent to the theoretical analysis presented in Fig. 3 and Table 1, where R1234yf and R410A, after R744 and R404A, had the largest potential for increase in refrigerant effect ($\Delta q/q$). Both R134a and R1234yf showed similar increments in saturation ($\Delta T_{c,sat,in}$) and exit ($\Delta T_{c,out}$) temperature in the condenser (Table 4) and, although the latter was developed to replace the former as a drop-in solution, the R1234yf has a larger potential to benefit from subcooling due to a smaller latent heat of vaporization than the R134a. Table 4 also shows the area occupied by subcooled liquid at COP maximizing subcooling, relative to the total heat transfer area. According to the model, if a subcooler was to be designed, the R1234yf would require the largest heat transfer area for COP maximizing subcooling conditions, within the four refrigerants considered.

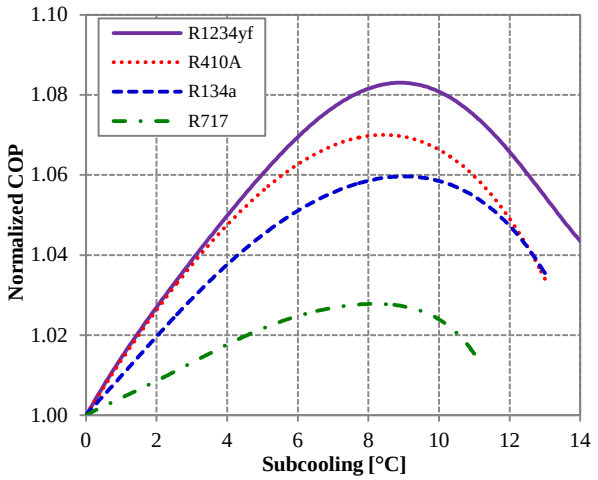

Figure 7: Effect of condenser subcooling on normalized COP for R717, R134a, R410A and R1234yf, at outdoor and indoor temperatures of 35°C and 27°C

Table 4: Summary of simulation results at condenser and evaporator air inlet temperature of 35°C and 27°C, respectively.

		R1234yf	R410A	R134a	R717
Maximum COP increase	[-]	8.4%	7.0%	5.9%	2.7%
COP maximizing subcooling	[°C]	8.9	8.5	8.9	8.4
Optimum subcooling area	[-]	18%	16%	14%	7%
$\Delta T^{*}_{c,sat,in}$	[°C]	0.9	1.1	0.9	0.4
$\Delta T^{*}_{c,out}$	[°C]	-7.1	-7.6	-7.4	-8.5
$T^{**}_{c,sat,avg}$	[°C]	46.7	45.7	46.7	45.5
$\Delta w^{*} / w^{**}$	[-]	1.8%	2.4%	1.9%	1.2%
$\Delta q^{*} / q^{**}$	[-]	10.3%	9.5%	8.0%	3.9%

* Between zero and COP maximizing subcooling conditions.
** At zero subcooling condition.

In order to include subcritical R744 in the simulation analysis, air inlet temperature was reduced to 14°C in the condenser, while in the evaporator it was lowered to 0°C. Although less realistic, this operating condition allows R744 to be compared with other fluids in terms of potential for COP increase with subcooling. Fig. 8 shows the normalized COP as a function of the condenser subcooling for R744, R410A, and R717. The cooling capacity was fixed at 4 kW. Although the three refrigerants are very distinct in terms of thermodynamic properties, i.e. liquid specific heat and latent heat of vaporization, they all showed similar values of COP maximizing subcooling, around 8°C. Maximum COP improvement, however, is by far the largest for R744 (about 12%), followed by R410A (4.4%) and R717 (2.4%). The improvements are consistent to the thermodynamic analysis presented in Fig. 3, where R744 showed the largest potential for increase in refrigerating effect and R717, the lowest.

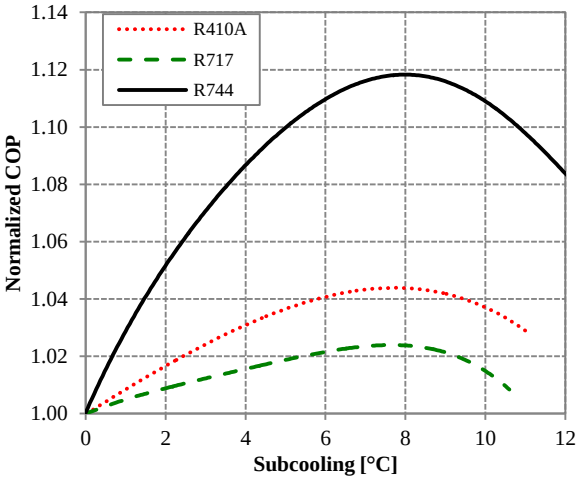

Figure 8: Effect of condenser subcooling on normalized COP for R744, R410A and R717, at outdoor and indoor temperatures of 35°C and 27°C

Differences between refrigerants also lied on the area occupied by subcooled liquid in COP maximizing subcooling conditions. R744 would require the largest subcooling area ratio (24%), followed by R410A (11%) and R717 (6%).

4. EXPERIMENTAL METHODS

The system chosen was a modified 2007 production line R134a automotive air-conditioning (AC) system. The compressor has a fixed displacement of 214 cm^3/REV and is connected through the same shaft to an electrically-driven motor with variable speed capability. The condenser is a parallel cross-flow microchannel heat exchanger with a face area of 0.24 m^2, depth of 16 mm, 18 louvered fins per inch and a total of 39 parallel microchannels tubes. Its pass-arrangement comprises a single-slab and two passes, the first with 26 channels and the second with 13 channels. The original evaporator, a plate-and-fin type, was maintained together with the original heating ventilation air conditioning (HVAC) module. The system setup (Fig. 9) with high-side liquid receiver and electronic expansion valve was found to be appropriate since changes in valve opening and refrigerant charge allow a convenient way to vary the condenser subcooling, once the receiver is completely filled with liquid.

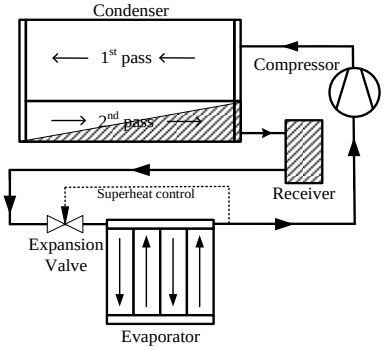

Figure 9: System setup

The experimental facility comprises the two environmental chambers and the refrigeration circuit. The condenser was installed at the inlet of an open-loop wind tunnel inside the outdoor chamber. The evaporator together with HVAC module was attached to the open-loop wind tunnel of the indoor chamber. In both chambers, a set of PID-controlled electrical heaters were used to control the air inlet temperature to the heat exchangers. In the outdoor chamber, an external chilled water coil removed the energy dissipated by condenser and electrical heaters. A dehumidifier was able to keep dew-point temperatures low enough for fully dry-conditions in the evaporator. The air flow rates were controlled with variable speed blowers. Air-side pressure drop across the flow nozzles was measured by differential pressure transducers while Type-T thermocouples measured the dry-bulb air temperature at the nozzle exits, in order to obtain the air flow rates. T-type thermocouple grids were installed upstream and downstream of evaporator and condenser to measure the dry-bulb temperatures. In the evaporator wind-tunnel, chilled-mirror dew-point sensors were also installed. Type-T immersed thermocouples and absolute pressure transducers were conveniently placed throughout the refrigeration circuit. In order to measure refrigerant mass flow rate, a Coriolis-type mass flow meter was installed between the liquid receiver and the expansion valve.

The calculated air flow rate combined with dry-bulb and dew-point temperature readings were used to obtain the cooling capacity on the air side of the evaporator. In addition, the cooling capacity was independently obtained by an energy balance on the refrigerant side, using mass flow rate and enthalpies obtained from pressure and temperature readings. The compressor power was obtained using measurements from a torque transducer and a tachometer mounted in the shaft that connects the compressor to the electrical motor. An uncertainty propagation analysis carried out in EES (2007) revealed an experimental uncertainty of ±6% for the cooling capacity obtained from the air-side, ±3% for that obtained from the refrigerant side and ±5% for the COP calculated with the cooling capacity on the refrigerant-side. Air and refrigerant side cooling capacities agreed within ±3%.

5. EXPERIMENTAL RESULTS

In this section, the effect of the condenser subcooling on the performance of the vehicular AC system operating with R134a and R1234yf is experimentally investigated. Since the R1234yf was designed to replace the R134a as a drop-in substance in automotive air conditioning systems, both refrigerants were conveniently tested in the same system and operating conditions. During the experiments, the air temperature and face velocity at the evaporator inlet were maintained at 30°C and 2.6 m/s, respectively. At the condenser inlet, the air face velocity was kept at 1.5 m/s and the air temperature, at 35°C. In order to vary the condenser subcooling, refrigerant mass was added in increments after the liquid receiver was completely filled with liquid so that subcooled liquid would accumulate towards the condenser exit. For each value of subcooling, data was taken during 15 minutes in steady-state. The evaporator exit superheat was maintained at 10±1°C by varying the opening of the electronic expansion valve accordingly.

In order for COP to be the only measure of improvement as condenser subcooling was varied, the cooling capacity obtained from the air side was maintained at an average of 4.1 kW, with deviations of ±0.3%. The control of the cooling capacity was carried out by carefully changing the compressor speed.

Fig. 10 displays infrared images of the condenser frontal surface at various degrees of subcooling, for R1234yf. The dashed-lines are an attempt to separate liquid subcooling from two-phase/desuperheating regions. Figs. 11 to 14 show the results for several system performance variables as a function of the condenser subcooling for both R134a and R1234yf. Continuous and dashed lines in the charts indicate a curve fitting of the experimental points.

Since the results in Figs. 10 to 14 are inter-related, they will be analyzed simultaneously. As mass of refrigerant accumulates in the form of subcooled liquid at condenser exit, the two-phase region is reduced, as illustrated by the infrared images of the condenser frontal surface (Fig. 10). This yields an increase in saturation temperature (Fig. 11) while the liquid refrigerant exiting the condenser is cooled below saturation temperature (Fig. 11). The increase in subcooling is a result of both reduction of condenser exit temperature and increase of saturation temperature.

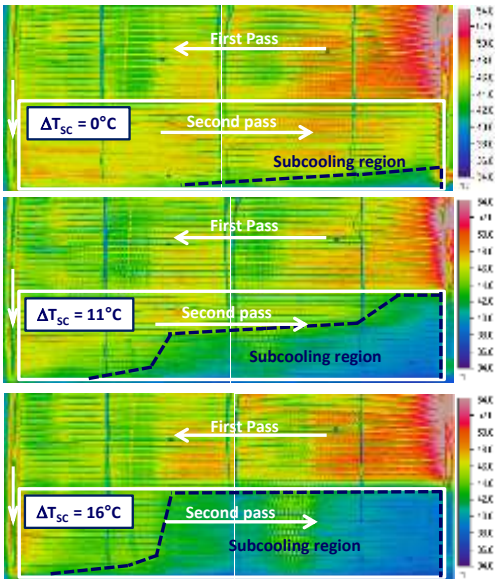

Figure 10: Infrared images at the inlet surface of the condenser for various degrees of subcooling with dashed lines to approximately indicate the area occupied the subcooled liquid (experimental).

Fig. 11 shows that the COP undergoes a maximum for both refrigerants at similar values of subcooling, i.e. about 9°C for R134a and around 11°C for R1234yf. The maximum COP is a result of the trade-off between increasing enthalpy difference through evaporator (Fig. 12) and specific work (isentropic) of compression (Fig. 12), as previously pointed out during the numerical study. The enthalpy at the evaporator inlet is reduced while the refrigerant exiting the condenser is subcooled, thus enlarging the enthalpy difference across the evaporator (Fig. 12), for both refrigerants. The specific isentropic work of compression, however, first decreases at lower values of subcooling due to a reduction of the pressure ratio (Fig. 13) and an increase in the compressor inlet pressure (Fig. 14) even though the condensing pressure increases (Fig. 11). This means that within lower values of subcooling the effect of the suction pressure increase (Fig. 14) on the pressure ratio is dominant over that of the condensing pressure increase (Fig. 11). At higher values of subcooling, however, as the condensing pressure rises sharply its effect becomes dominant over that of the compressor inlet pressure decrease, thus elevating the pressure ratio (Fig. 13) and consequently the isentropic specific work of compression. It can be seen at Fig. 13 that the isentropic efficiency reaches a maximum for both fluids, even though variations are small. The variations in the isentropic efficiency are caused by changes in pressure ratio (Fig. 13) and compressor speed while matching the cooling capacity at different values of subcooling.

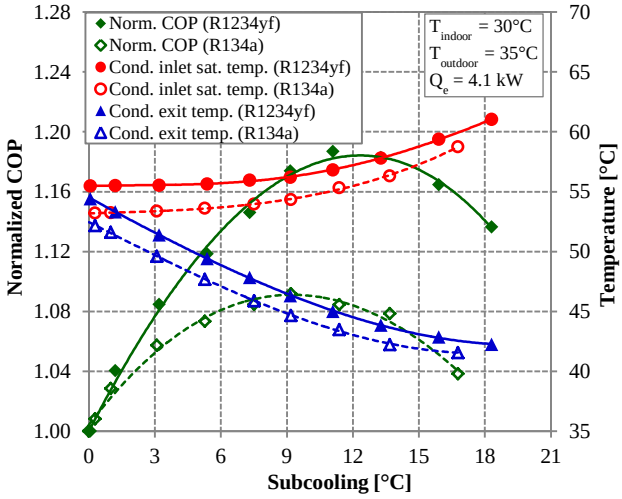

Figure 11: Effect of condenser subcooling on normalized COP, inlet saturation and exit temperatures of the refrigerant in the condenser for R134a and R1234yf (experimental).

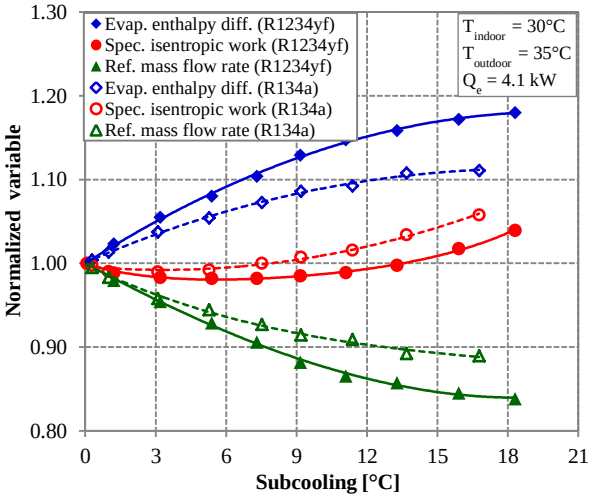

Figure 12: Effect of condenser subcooling on normalized refrigerant enthalpy difference across the evaporator, specific isentropic compression work and refrigerant mass flow rate, for R134a and R1234yf (experimental)

Since the capacity was kept constant for each subcooling and the enthalpy difference across the evaporator increases with subcooling (Fig. 12), the refrigerant mass flow rate is significantly reduced (Fig. 12), as also discussed in the numerical study. As a consequence, refrigerant-side pressure drops across the system are reduced dramatically, as shown in Fig. 14 for suction line, evaporator and condenser (R1234yf only). In the condenser, the growth of the subcooled region also contributes to the decrease in pressure drop, as previously discussed. In the evaporator, an additional contribution to the pressure drop reduction is given by lower inlet qualities to the coil.

Fig. 14 confirms that the performance of the condenser in terms of saturation temperature is dramatically worsened with the increase in subcooling because the subcooled region introduces an area with lower temperature difference and heat transfer coefficient, as pointed out during the numerical study and illustrated by the infrared images (Fig. 10). The evaporator performance in terms of exit saturation temperature, however, does not seem to be affected (Fig. 14), even though the refrigerant side pressure drop (Fig. 14) decreased significantly.

Results in Figs. 11 and 12 confirmed that R134a and R1234yf respond differently to variations in condenser subcooling. According to Fig. 11, the COP of the R134a system was improved by 9% while for R1234yf the COP increased up to 19%. These results are consistent to the numerical analysis which demonstrated that the condenser subcooling can be more beneficial for R1234yf systems than for R134a systems. The reasons for these differences are explained next. First, Fig. 12 shows that refrigerant enthalpy difference across the evaporator of the R1234yf system is in fact more sensitive to condenser subcooling than that of the R134a. Between zero and COP maximizing subcooling, the relative gain in refrigerating effect with subcooling of R1234yf was equal to 15% while for R134a it was only 8%. R1234yf (163 kJ/kg) has a smaller latent heat of vaporization ($h_{fg,e}$) than R134a (199 kJ/kg) but almost

equal liquid specific heats. So according to Eq. (3), the R1234yf would benefit more from cooling the refrigerant at the condenser exit. In addition, Fig. 11 shows that, between zero and COP maximizing subcooling, the decrease in the refrigerant exit temperature ($\Delta T_{c,out}$) is greater for R1234yf (-9.3°C) than for R134a (-7.7°C). Additional differences in COP improvement between the two refrigerants are related to specific isentropic compression work (Fig. 12), which decreased by 1% for R1234yf and increase by 1.5% for R134a, between zero and COP maximizing subcooling. Since the sensitivity of isentropic compression work to increments in condensing temperature is very similar between the two refrigerants (Fig. 4) and both of them showed similar increases in saturation temperature (Fig. 11), this difference is probably associated with relative increase in compressor inlet pressure with subcooling, which is more substantial for R1234yf than for R134a.

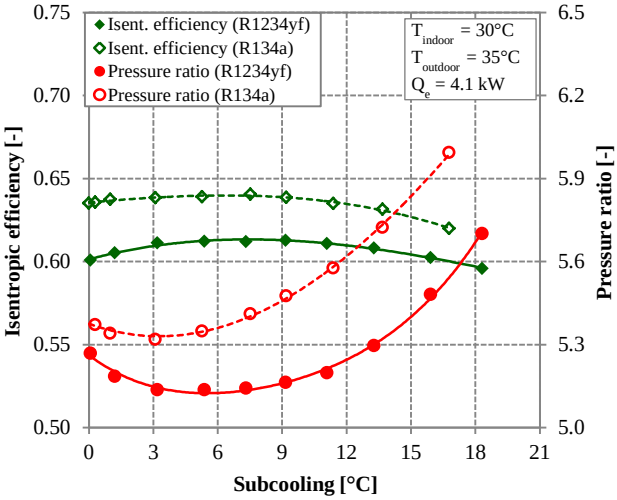

Figure 13: Effect of condenser subcooling on isentropic efficiency and compressor pressure ratio for R134a and R1234yf (experimental).

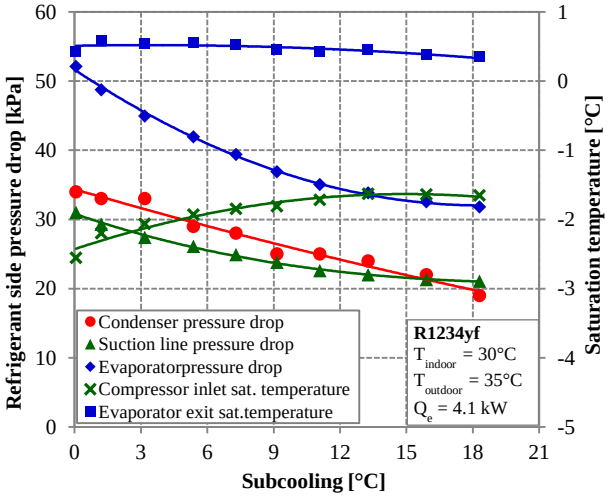

Figure 14: Effect of condenser subcooling on refrigerant side pressure drops and saturation temperatures (at the evaporator exit and compressor inlet) for R1234yf (experimental).

6. CONCLUSIONS

A theoretical and experimental study about the effect of condenser subcooling on the performance of vapor-compression systems has been presented probably for the first time in the open literature, to the best of the authors' knowledge. This study showed that, as condenser subcooling increases, the COP undergoes a maximum as a result of a trade-off between increasing refrigerating effect, due to the reduction of the condenser exit temperature, and increasing specific compression work, due to the increase in the condensing pressure. The increase in condensing pressure was associated with the reduction of the air-refrigerant temperature difference and the refrigerant-side heat transfer coefficient once the two-phase region in the condenser is shrunken to accommodate the subcooled liquid region. This paper also showed that the thermodynamic properties associated with the relative increase in refrigerating effect, i.e. liquid specific heat and latent heat of vaporization, are dominant to determine the maximum COP improvement with condenser subcooling. Refrigerants with large latent heat of vaporization, such as R717 and R718, tend to benefit the least from condenser subcooling. For a typical AC system, simulation results indicated that R1234yf would benefit the most from condenser subcooling in comparison to R410A, R134a and R717 due to its smaller latent heat of vaporization. In a different operating condition, results revealed that subcritical R744 would have significantly higher potential for COP improvement with subcooling than R410A and R717. In addition it has been concluded that the COP maximizing subcooling does not seem to be strong function of the thermodynamic properties for the same system under identical operating conditions.

An experimental study based on R134a and R1234yf in a vehicular AC system confirmed the trends observed during the numerical analysis. For both refrigerants, it was experimentally demonstrated that the COP in fact undergoes a maximum as condenser subcooling is varied. It has also been confirmed that the COP of the system operating with R1234yf can benefit more from the condenser subcooling than that with R134a due differences in thermodynamic properties (latent heat of vaporization). Experimentally measured COP improvements due to condenser subcooling were, however, much larger than those observed during the numerical study for reasons to be revealed in a next paper.

NOMENCLATURE

COP	coefficient of performance	(-)	**Subscripts**	
h	enthalpy	(kJ kg^{-1})	avg	average
q	enthalpy difference across the evaporator	(kJ kg^{-1})	c	condenser
SH	superheated vapor region	(-)	e	evaporator
SC	subcooled liquid region	(-)	fg	liquid-vapor
T	temperature	(°C)	in	inlet
TP	two-phase region	(-)	out	outlet
w	specific compression work	(kJ kg^{-1} K^{-1})	sat	saturation
			sub	subcooling

REFERENCES

Cavallini, A., Del Col, D., Doretti, L., Matkovic, M., Rossetto L. and Zilio C., 2005. Condensation heat transfer and pressure gradient inside multiport minichannels, *Heat Transfer Engineering* 27, 45-55

Chang, Y.J., Wang, C.C., 1997. A generalized heat transfer correlation for louver fin geometry, *International Journal of Refrigeration* 40, 533-544

Churchill, S.W., 1977. Friction-factor equation spans all fluid-flow regimes, *Chemical Engineering* 84.

Corberan, J.M., Martinez, I.O., Gonzalves, J., 2008. Charge optmisation study of a reversible water-to-water propane heat pump, *International Journal of Refrigeration* 31, 716-726

Couvillion R.J., Larson, M.W., Somerville, M.H., 1988. Analysis of a vapo-compression refrigeration system with mechanical subcooling, *ASHRAE Transactions* 94 ,641-659.

Domanski, P.A., Didion, D.A., 1994. Evaluation of suction-line/liquid-line heat exchange in the refrigeration cycle, *International Journal of Refrigeration* 17, 487-493.

EES, 2007. Engineering Equation Solver. Academic Professional Version 7.934-3D, F-Chart Software, Middleton, WI, USA.

Friedel, L., 1979. Improved friction pressure drop correlations for horizontal and vertical two phase pipe flow. *In: European Two Phase Flow Group Meeting*, Italy, Paper E2.

Gnielinski, V., 1976. New equations for heat and mass transfer in turbulent pipe and channel flow, International *Chemical Engineering* 16, 359–368.

Gosney, W.B., 1982. Principles of Refrigeration, *Cambridge University Press*, New York, NY.

Gungor K.E., Winterton R.H.S., 1986. A general correlation for flow boiling in tubes and annuli, International *Journal of Heat and Mass Transfer* 29, 351-358

Hrnjak, P., Litch, A.D., 2008. Microchannel heat exchangers for charge minimization in air-cooled ammonia condensers and chillers, *International Journal of Refrigeration* 31, 658-668.

Incropera, F.P., DeWitt, D.P., Bergman, T.L., Lavine, A.S., 2006. Fundamentals of Heat and Mass Transfer. John Wiley & Sons, Hoboken, NJ.

Linton, J.W., Snelson, W.K., Hearty, P. F., 1992. Effect of condenser liquid subcooling on system performance for refrigerants CFC-12, HFC-134a and HFC-152a. *ASHRAE Transactions* 98, 160-146

Peterson G.E., 1997. Condensate liquid management system for air conditioner. US Patent No 5,682,757

Pomme, V., 1999. Improved Automotive A/C Systems Using a New Forced Subcooling Technique. *SAE International Congress & Exposition*, Detroit, MI paper 1999-01-1192

Primal, F., Lundqvist, P., 2005. Refrigeration systems with minimized refrigerant charge: system design and performance. *In: Proceedings of the IMechE 219 Part E: Journal of Process Mechanical Engineering*, 127-138

Radermacher, R., Yang, B., Hwang, Y., 2007. Integrating Alternative And Conventional Cooling Technologies, *ASHRAE Journal*, October 2007, 28-35

Yamanaka Y, Matsuo H, Tuzuki K, Tsuboko T, 1997, Development of Sub-cool system, *SAE Technical Paper Series*, paper 970110

ACKNOWLEDGEMENT

The authors are thankful for the support provided by the Air Conditioning and Refrigeration Center at the University of Illinois at Urbana-Champaign and by the CNPq agency in Brazil.